Structure and Chemical Bonding in $K_{14}Cd_9Tl_{21}$, a Compound Containing Both Isolated Tl_{11}^{7-} Clusters and $^2_\infty[Cd_9Tl_{10}^{7-}]$ Metallic Layers

Monique Tillard-Charbonnel,* Abdelkrim Chahine, Claude Belin, Roger Rousseau, and Enric Canadell*

Abstract: The compound $K_{14}Cd_9Tl_{21}$ has been prepared by fusion of the elements in a tantalum reactor followed by slow cooling at the rate of 6° per hour to enable crystal growth. The X-ray crystal structure (hexagonal, $P\bar{6}2m$; $a = 9.884(3)$, $c = 17.173(5)$ Å; $Z = 2$) was refined to reliability factors of $R1 = 5.09$, $wR2 = 11.64\%$. The anionic substructure contains both isolated clusters of Tl_{11}^{7-} and a layered network based on Cd_5Tl_2 pentagonal bipyramids. The structure–electron count relationship for the Tl_{11}^{7-} cluster was analyzed in detail. The $Cd_9Tl_{10}^{7-}$ layers are found to confer metallic properties to the material, and the bonding within such layers is found to be highly delocalized.

Keywords
cadmium · clusters · layered compounds · semiempirical calculations · thallium · Zintl phases

Introduction

Investigations within alkali metal–Group 13 element systems have uncovered an interesting field in solid-state chemistry with numerous intermetallic phases displaying novel and original structures. In such systems, the electronegative elements are able to adapt their bonding and coordination to fit a wide range of electron counts.

Previous reports have shown intermetallic compounds of gallium to be on the borderline between metallic phases and valence compounds, for which the octet and the $(8 - N)$ rules hold (Zintl phases). Like boron, gallium behaves in these compounds as a hypoelectronic element that needs to be reduced by the electropositive elements to form clusters, fused clusters, and various other fragments. Although isolated (naked) clusters remain rare in gallium intermetallic phases, Ga_6 and Ga_{11} have been found in Ba_5Ga_6[1] and Cs_8Ga_{11},[2] respectively, and numerous cluster frameworks may form, which can be very simple (as in K_3Ga_{13})[3] or very complicated in some ternary or quaternary phases (e.g., $Li_{38}(Zn_{0.337}Ga_{0.663})_{101}$[4]). In these networks, atom defections, atom substitutions, disorder, or nonstoichiometry often obscure the understanding of electronic and bonding requirements. Gallium intermetallic phases exhibit globally delocalized electrons, since coordination numbers within clusters are larger than the available bonding electron pairs. Nevertheless, these clusters have structures that are adapted to well-defined electron counts, which generally, but not always, conform to classical Wade's rules.[5] Anionic charges that are higher than would be required for naked clusters are generally alleviated by intercluster two-center two-electron classical bonding. Some gallium intermetallic phases, as for example Na_7Ga_{13} and $Na_{22}Ga_{39}$,[6–8] contain icosahedral clusters that have one or more non-*exo*-bonded atoms bearing lone electron pairs. These clusters may be regarded as intermediate steps towards the formation of naked anions. This richness in cluster and framework types within the alkali metal–gallium system[9] has sparked further research within the heavier Group 13 In and Tl systems in recent years.

Intermetallic compounds of indium can be divided into two groups, namely, phases exhibiting extended frameworks with two-center two-electron intercluster bonding (e.g., $A_3Na_{26}In_{48}$[10]) and phases containing naked clusters, having either classical electron counts, as in In_4^{8-} and In_5^{9-},[10] or hypoelectronic electron counts with respect to Wade's criterion,[5] as in In_{11}^{7-}[10,11] and the heteroatom-centered clusters $In_{10}Ni^{10-}$ and $In_{10}Zn^{8-}$.[10]

In contrast to indium and gallium phases, which tend to form cluster-based three-dimensional frameworks, alkali metal–thallium systems have been shown to be very rich in discrete clusters, such as, Tl_3^{7-},[12] Tl_4^{8-},[12,13] Tl_5^{7-},[10,14] Tl_6^{6-},[10] Tl_9^{9-},[14] Tl_{11}^{7-},[10,15] Tl_{13}^{10-},[10,16] Tl_{13}^{11-},[17] and $Tl_{12}Cd^{12-}$.[18] The pentacapped trigonal prismatic Tl_{11}^{7-} anion is the only unit found in A_8Tl_{11} (A = K, Rb, Cs) phases.[10,15] It is also present in $K_{18}Tl_{20}Au_3$,[19] but in conjunction with an analogous Au-substituted $Tl_9Au_2^{9-}$ anion. In $A_{15}Tl_{27}$,[20] layers of naked Tl_{11}^{7-}

[*] Dr. M. Tillard-Charbonnel, Dr. A. Chahine, Dr. C. Belin
Laboratoire des Agrégats Moléculaires et Matériaux Inorganiques
UPRESA CNRS 5072, Université de Montpellier 2
Sciences et Techniques du Languedoc, Place Eugène Bataillon
34095 Montpellier Cedex 5 (France)
Fax: Int. code + (4) 6714-3304
email: mtillard@univ-montp2.fr
Dr. E. Canadell, Dr. R. Rousseau
Institut de Ciéncia de Materials (CSIC)
Campus de la U. A. B., Bellaterra (Spain)
Fax: Int. code + (3) 580-5729
email: canadell@zas.qf.ub.es

  0947-6539/97/0305-0799 $ 17.50+.50/0

anions alternate with a two-dimensional $^{2}_{\infty}[Tl^{8-}_{16}]$ framework built from the condensation of Tl_{11} units.

In this article we report the detailed structural analysis of the ternary compound $K_{14}Cd_9Tl_{21}$, in which Tl^{7-}_{11} isolated clusters coexist with a two-dimensional network containing Cd_5Tl_2 pentagonal bipyramids.[21] Semiempirical EHT molecular orbital and tight-binding band structure calculations have been used to analyze the bonding in Tl^{7-}_{11} and the electronic structure of the 2D sublattice.

Experimental Section

Synthesis and data collection: The alloy KCdTl was prepared by fusion of the elements in equal proportions. The weld-sealed tantalum reactor was heated at 893 K for 12 h, and then cooled slowly at the rate of $6°h^{-1}$ to enable crystal growth. The compound $K_{14}Cd_9Tl_{21}$ was obtained in relatively high yield in association with some KCd_{13} and K–Tl phases. A new synthesis with the elements in a ratio of 14:9:21 was carried out to confirm the stoichiometry of $K_{14}Cd_9Tl_{21}$. The product of the reaction was quite homogeneous and had a lustrous appearance, but it was very air sensitive and was examined under a microscope inside a glove box filled with dry argon. Selected crystals were tested by X-ray oscillation and Weissenberg techniques, and the one with the best diffracting properties, of dimensions $0.14 \times 0.105 \times 0.016$ mm^3, was used for intensity data collection (Table 1) on an Enraf Nonius CAD4 automatic diffractometer (graphite-monochromated $Mo_{K\alpha}$ radiation). Accurate lattice parameters, $a = b = 9.884(3)$ Å, $c = 17.173(5)$ Å, were determined by least-squares refinement of angular positions of 25 reflections ($8.6 \leq 2\theta \leq 28.9$) collected and automatically centered on the diffractometer. Profile analysis indicated that an $\omega-\theta$ scan method was the most appropriate for data collection. Scan ranges were calculated from the formula $A + B\tan\theta$, where A (taken as 1.2) depends upon the mosaic spread and B (taken as 0.35) allows for increasing peak width due to $K_{\alpha 1}$ and $K_{\alpha 2}$ splitting. 2938 reflections were measured at room temperature in the octant hkl of the hexagonal cell in the range $4 \leq 2\theta \leq 60°$ without any significant loss in the intensities of the three standard reflections checked every 100 recorded reflections. Data were corrected for background, Lorentz, and polarization effects, and after the composition of the crystal was known, for absorption ($\mu = 624.1$ cm^{-1}, transmission factors = 0.044–0.377), by using the procedure provided by the SHELX 76 program.[22] Intensities of equivalent reflections averaged well ($R_{int} = 4.95\%$) in the corresponding subgroup.

Table 1. Selected data collection and refinement parameters for $K_{14}Cd_9Tl_{21}$.

space group, Z	$P\bar{6}2m$ (no. 189), 1
lattice parameters (Å)	9.884(3), 9.884(3), 17.173(5)
λ (Å), 2θ limit (°)	0.71073, 60
abs. coeff. $Mo_{K\alpha}$ (cm^{-1})	624.10
range of transmission coeff.	0.3772–0.0367
no. of recorded rflns.	2938
no. of unique observed rflns., criterion	1037, $I > 3\sigma(I)$
no. of variables	48
$R1$ [a], $wR2$ [b] (%)	5.09, 11.64%
resid. electron densities (e Å^{-3})	+3.9 and −2.0

[a] $R1(F) = \sum||F_o| - |F_c||/\sum|F_o|$. [b] $wR2(F) = [\sum w(F_o - F_c)^2/\sum wF_o^2]^{1/2}$, where $w = 1/[\sigma^2(F_o^2) + (0.0734P)^2]$ with $P = (\max(F_o^2, 0) + 2F_c^2)/3$.

Electrical resistivity was measured for a single crystal by using a two-probe method (direct current: 10–100 mA, gold contacts) in the temperature range 218–323 K.

Structure solution and refinement: The structure of the ternary compound $K_{14}Cd_9Tl_{21}$[21] was solved in the noncentrosymmetric space group $P\bar{6}2m$ (no. 189) by the direct methods of SHELXS-86,[23] which allowed localization of all heavy atoms, and then refined using the program SHELX 76.[22] These results had been reported in a brief communication (further details of the crystal structure investigations may be obtained from the Fachinformationszentrum Karlsruhe, 76344 Eggenstein-Leopoldshafen (Germany) on quoting the depository number CSD-400782).[21] The initial structural refinement was improved using the program SHELXL 93.[24] Among the 2938 recorded reflections, 1830 non-zero were averaged into 1037 unique corresponding to the criterion $I > 3\sigma(I)$ used in the refinements. Full-matrix least-squares refinements of 48 parameters were carried out, and extinction corrections were applied. Final agreement factors were $R1 = 5.09\%$ and $wR2 = 11.64\%$. Refinement of site occupations of alkali metals while keeping Tl and Cd occupations fixed showed that, within the 3σ limit, the alkali metal sites are entirely occupied. By means of the same procedure, heavy atoms were also found to fully occupy their sites. Structural representations (Figures 1 and 3) clearly show the lack of inversion center. The absolute configuration of the noncentrosymmetric structure could be determined by means of the difference of nearly 2% in the $R1$ value upon inversion of positional parameters. Maximum residual densities in the last Fourier difference ranged from +3.9 to −2.0 e Å^{-3}. The crystallographic formula $K_{14}Cd_9Tl_{21}$ was found to be in good agreement with the formula gained from flame chemical analysis of X-ray-checked single crystals (K/Cd/Tl ratio of 0.662(6):0.435(3):1).

Results and Discussion

Structural description: $K_{14}Cd_9Tl_{21}$ (Figure 1) fits in well with the structural family of phases containing both discrete clusters and two-dimensional frameworks. The naked Tl^{7-}_{11} cluster is indeed the same as that recently found in $A_{15}Tl_{27}$ (A = Rb, Cs),[20] but $K_{14}Cd_9Tl_{21}$ differs in its metallic layer, which is formulated $^{2}_{\infty}[Cd_9Tl^{7-}_{10}]$ instead of $^{2}_{\infty}[Tl^{8-}_{16}]$ in the former. Packed

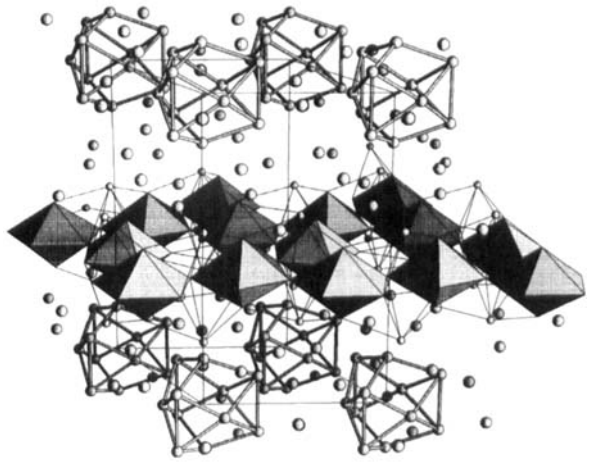

Figure 1. Representation of layered packing in the $K_{14}Cd_9Tl_{21}$ structure, approximately viewed along [1 2 0].

Abstract in French: *Le composé $K_{14}Cd_9Tl_{21}$ a été préparé par fusion directe des éléments dans un réacteur en tantale scellé sous argon. Des monocristaux ont été obtenus par refroidissement lent ($6°hr^{-1}$). La structure cristalline ($P\bar{6}2m$; $a = 9.884(3)$, $c = 17.173(5)$ Å; $Z = 2$, $R1 = 5.09$ et $wR2 = 11.64\%$) est constituée de trois couches: clusters isolés Tl^{7-}_{11}, cations K^+ et un feuillet formé de bipyramides pentagonales Cd_5Tl_2. Une analyse détaillée de la relation entre structure et décompte électronique est présentée pour l'anion Tl^{7-}_{11}. Avec une liaison chimique très délocalisée, les feuillets $Cd_9Tl^{7-}_{10}$ confèrent au matériau des propriétés métalliques.*

0947-6539/97/0305-0800 $ 17.50+.50/0 Chem. Eur. J. 1997, 3, No. 5

ing in both structures results from the alternation (along z axis) of layers of Tl_{11}^{7-} discrete clusters and layers of metal condensed clusters separated by seams of potassium cations.

Atoms Tl(2), Tl(3), and Tl(4) form the Tl_{11}^{7-} anion (Figure 2, Table 2) which can be regarded as having the geometry of a flattened pentacapped trigonal prism; the Tl(4) atoms form an enlarged prism with the rectangular and triangular faces capped by Tl(2) and Tl(3) atoms, respectively. The distortion (compression along the 3-fold axis) from a regular pentacapped prism (Tl_{11}^{9-}) considerably increases the Tl(4)–Tl(4) length within the base of the prism (from 3.10 to 5.03 Å) leading to the loss of six bonds per Tl_{11} unit.

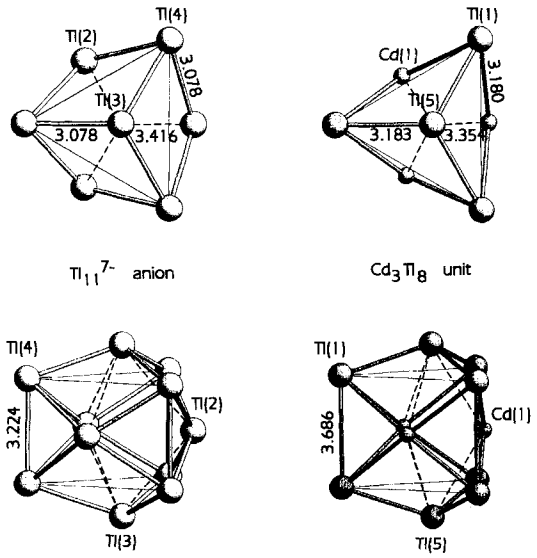

Figure 2. Representations of the Tl_{11}^{7-} anion (left) and of the Cd_3Tl_8 unit (right). The edges of the prism base are represented by thin lines (Tl(4)–Tl(4) = 5.035 Å in Tl_{11}^{7-} and Tl(1)–Tl(1) = 5.234 Å in the Cd_3Tl_8 unit). Dashed lines represent long Tl–Tl (3.416 Å) and Cd–Tl (3.354 Å) distances in Tl_{11}^{7-} and Cd_3Tl_8, respectively. For clarity, Cd(1)–Cd(1) distances (3.083 Å) are not indicated in the representations of Cd_3Tl_8.

Table 2. Principal interatomic distances (Å) in $K_{14}Cd_9Tl_{21}$

Tl(1)		Cd(2)	2.964(3)	Tl(3)	3	Tl(4)	3.078(2)
	2	Cd(1)	3.180(3)		3	Tl(2)	3.416(2)
	2	Tl(5)	3.183(1)		3	K(2)	3.776(9)
	2	Cd(1)	3.244(2)		3	K(1)	3.90(1)
		K(1)	3.581(8)				
		K(2)	3.671(9)	Tl(4)		Tl(3)	3.078(2)
		Tl(1)	3.686(3)		2	Tl(2)	3.078(1)
	2	K(2)	3.691(4)			Tl(4)	3.224(3)
						K(1)	3.478(9)
Tl(2)	4	Tl(4)	3.078(1)		2	K(1)	3.815(7)
	2	Tl(3)	3.416(2)		2	K(3)	3.858(1)
	2	K(1)	3.580(8)			K(2)	3.864(9)
	2	K(3)	3.966(2)				
				Cd(1)		Cd(1)	2.961(6)
Tl(5)	3	Tl(1)	3.183(1)			Cd(2)	2.997(4)
	3	Cd(1)	3.354(2)		2	Cd(1)	3.083(5)
	3	K(2)	3.767(6)		2	Tl(1)	3.180(3)
	3	K(1)	3.995(6)		2	Tl(1)	3.244(2)
					2	Tl(5)	3.354(2)
K(1)		Tl(4)	3.478(9)		2	K(2)	3.703(8)
		Tl(1)	3.581(8)				
		Tl(2)	3.580(8)	Cd(2)	2	Cd(2)	2.816(7)
	2	Tl(4)	3.815(7)		2	Tl(1)	2.964(3)
		Tl(3)	3.90(1)		2	Cd(1)	2.997(4)
	2	Tl(5)	3.995(6)		4	K(2)	3.825(8)
	2	K(2)	4.095(9)				
		K(2)	4.20(1)	K(2)		Tl(1)	3.671(9)
		K(3)	4.395(6)		2	Tl(1)	3.691(4)
					2	Cd(1)	3.703(8)
K(3)	6	Tl(4)	3.858(1)		2	Tl(5)	3.767(6)
	3	Tl(2)	3.966(2)			Tl(3)	3.776(9)
	3	K(1)	4.395(6)		2	Cd(2)	3.825(8)
						Tl(4)	3.864(9)
						K(1)	4.095(9)

In the experimental cluster, there are three types of short distances, namely, that between equatorial cap and prism vertex (Tl(2)–Tl(4) = 3.078 Å), that between apical cap and prism vertex (Tl(3)–Tl(4) = 3.078 Å), and the height of the trigonal prism (Tl(4)–Tl(4) = 3.224 Å). These distances should be compared with the single Tl–Tl bond length of 3.09 Å given by Pauling.[25] Furthermore, there might well be some bonding interaction between equatorial Tl(2) and apical Tl(3), since these atoms are separated by 3.416 Å (bond order of 0.29 according to Pauling's formula). We discuss these findings in the last section of the article, where we also establish the correlation between electron count and the geometrical distortion from regular to experimental pentacapped prism.

Molecular calculations clearly show (see next section) that the Tl_{11} cluster has a valence electron count of 40 (closed-shell configuration), including a -7 anionic charge. By assuming the complete ionization of potassium atoms and using formal charges, the compound can be then formulated as $14K^+$, Tl_{11}^{7-}, $[Cd_9Tl_{10}]^{7-}$.

The two-dimensional layer $^2_\infty[Cd_9Tl_{10}^{7-}]$ can be visualized (Figure 3a) as a network containing Cd_5Tl_2 pentagonal bipyramids: five-membered planar rings of cadmium atoms ($4 \times$ Cd(1) and $1 \times$ Cd(2)) are capped on each side by Tl(1) atoms; these bipyramids are condensed by apex-sharing of Cd(1) and by three-center direct *exo*-bonding (Cd(2)–Cd(2)). Within the pentagonal base, Cd–Cd bonds range from 2.961 to 3.083 Å, while the *exo* bond length is 2.816 Å (Pauling's Cd–Cd single bond is 2.83 Å). Moreover, each trimeric unit of pentagonal bipyramids is

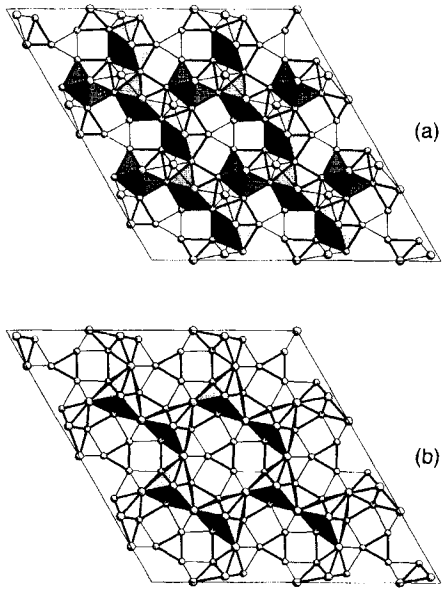

Figure 3. Representation of the $^2_\infty[Cd_9Tl_{10}^{7-}]$ two-dimensional layer projected onto the z axis, depicted as a) condensed pentagonal Cd_5Tl_2 bipyramids with each trimeric unit capped by two Tl(5) atoms on the three-fold axis, and b) condensed Cd_3Tl_8 units geometrically related to the Tl_{11}^{7-} anion.

capped on each side (along the three-fold axis) by two additional thallium atoms (Tl(5)). Within the layer, the Cd–Tl distances range from 2.964 to 3.354 Å (Pauling's single-bond length Cd–Tl is 2.92 Å), and the distance between the two capping thallium atoms Tl(1) and Tl(5) is 3.183 Å. All these distances indicate that there is some electron delocalization.

An alternative description of the structure would be to consider the two-dimensional layer $^{2}_{\infty}[Cd_9Tl^{7-}_{10}]$ as condensed Cd_3Tl_8 units (Figure 3b) with a geometry close to that adopted by the Tl_{11}-based units in $A_{15}Tl_{27}$. The Cd_3Tl_8 units (see Figure 2) are fused by Tl(1)–Tl(1) edge-sharing (along the z axis) and by two-center bridges between equatorial Cd(1) caps of adjacent units (Cd(1)–Cd(1) = 2.961 Å). The major difference in the arrangement of M_{11} units in $K_{14}Cd_9Tl_{21}$ and $A_{15}Tl_{27}$ is the occupation of the (0, 0, 1/2) crystallographic site, at the center of the $[M_{11}]_6$ ring, by a $[Cd(2)]_3$ triangular unit in the former and a large alkali cation (Rb, Cs) in the latter. In $K_{14}Cd_9Tl_{21}$, each Cd(2) atom is connected to two Cd_3Tl_8 units by the Cd(1) cap and by the prism vertex atoms Tl(1) (2 × Cd(2)–Cd(1) bonds of 2.997 Å and 2 × Cd(2)–Tl(1) bonds of 2.964 Å). Within the Cd_3Tl_8 unit, the Cd(1) capping atom lies closer to the rectangular face of the trigonal prism than does the Tl(2) atom in the discrete Tl^{7-}_{11} anionic moiety. The flattening occuring at this capping atom is reflected by the equatorial cap-to-equatorial cap Cd(1)–Cd(1) distance of 3.083 Å (the Tl(2)–Tl(2) distance is 3.785 Å in Tl^{7-}_{11}). Within the central triangular unit, Cd(2)–Cd(2) distances are even shorter (2.816 Å) and close to the Cd–Cd single-bond length of 2.83 Å.

Electronic structure: From the standpoint of electronic structure, the $K_{14}Cd_9Tl_{21}$ system may be regarded as consisting of three separate units, the first of which is the sheet consisting of K^+ ions. As this sheet is essentially composed of closed-shell cations, it is of little interest from the molecular orbital perspective. The second structural motif is that of the isolated eleven-atom thallium cluster, which is of interest because its geometry is not that of the regular Wade polyhedron. This fact raises questions regarding the skeletal electron count and the factors favoring this geometry. The third structural element is the Cd_9Tl_{10} sheet. Once an electron count has been established. the question of whether it is metallic or insulating may then be addressed. Also, it would be interesting to know whether the sheet can be viewed as a series of condensed Cd–Tl clusters, as suggested in the previous section, or whether it must be viewed as a continuous delocalized network. The focus of this section will be to address these issues in order to provide as complete a conceptual picture of $K_{14}Cd_9Tl_{21}$ as possible. The system was examined by performing Extended Hückel molecular orbital and tight-binding band-structure calculations[26] on the various elements. The orbital exponents and parameters used were those collected in Table 3. Preliminary tests showed that the role of the Cd 4d orbitals was negligible, so that they were not included in the computations reported here. Two quite different sets of parameters for Tl have been used in the literature.[27, 28] All the results reported in the following were obtained by using those of reference [24] (set 1 in Table 3). However, as discussed below, the main results of our study were checked by repeating the calculations with the Tl parameters of reference [25] (set 2 in Table 3).

Table 3. Exponents and parameters used in the calculations.

Atom	Orbital	H_{ii}, eV	ζ
Tl set 1 [a]	6s	−11.60	2.30
	6p	−5.80	1.60
Tl set 2 [b]	6s	−16.20	2.37
	6p	−9.00	1.97
Cd [c]	5s	−12.50	2.30
	5p	−6.60	2.10
K [d]	4s	−4.34	0.874
	4p	−2.73	0.874

[a] From ref. [27]. [b] From ref. [28]. [c] From ref. [29]. [d] From ref. [36].

A. The Tl_{11} cluster: The first subject of interest is the correlation between electron count and structure for the eleven-atom thallium cluster. Previous papers have dealt with this problem.[30, 32] Sevov and Corbett[30a] were the first to assign an electron count of 40 valence electrons to an identical In_{11} cluster. This count is lowered to 38 for the $Tl_9Au^{9-}_2$ analogue,[19] which undergoes a compression along the threefold axis, leading to a transannular Au–Au bond and an uncommon nonconvex polyhedron. They rationalized this count based on extended Hückel calculations and HOMO–LUMO gaps. In principle, the electron count for an ideal eleven-atom cluster with a pentacapped trigonal prismatic geometry (D_{3h}) can easily be obtained by viewing this cluster as being a tricapped trigonal prism, which is a *closo* deltahedron, capped with two additional atoms. According to the classical counting rules for deltahedral clusters, this capping will not change the number of *skeletal* electron pairs, which, according to the Wade rules, is 10. In the present case this would lead us to a total of (10+11) valence electron pairs for the Tl_{11} cluster, which exceeds the above-mentioned electron count of 40 by two electrons. Sevov and Corbett showed[30a] by means of a molecular orbital correlation diagram that a distortion from the idealized bicapped deltahedral geometry to the experimentally observed one produces a lower skeletal electron count by raising one orbital from the bonding to the antibonding region. Although this study was quite clear, a slightly more in-depth investigation will be presented here to provide further insight into the nature of the electron count and cluster geometry, related to that of an idealized bicapped deltahedron.

To begin the study of electron count and geometric relations, a molecular orbital correlation diagram for a distortion of the Tl_{11} cluster from the idealized pentacapped trigonal prismatic cluster (all Tl–Tl bond lengths are 3.10 Å) to the observed experimental geometry of the Tl_{11} cluster in $K_{14}Cd_9Tl_{21}$ is presented in Figure 4. This diagram is essentially identical to that reported by Sevov and Corbett[30a] for In_{11}. The only significant change along this distortion coordinate is the raising of an a'_1 orbital from the bonding manifold to the antibonding manifold. This process provides the rationale for the −7 charge on the cluster as opposed to the −9 charge predicted by use of the Wade rules and the capping principle. Distortion of this cluster may be viewed as involving two fundamental geometrical changes, the first of which is the breaking of the six Tl(4)–Tl(4) bonds in the capped triangular faces of the ideal cluster. In terms of orbitals we may assume that it will require the breaking of

0947-6539/97/0305-0802 $ 17.50+.50/0 Chem. Eur. J. 1997, 3, No. 5

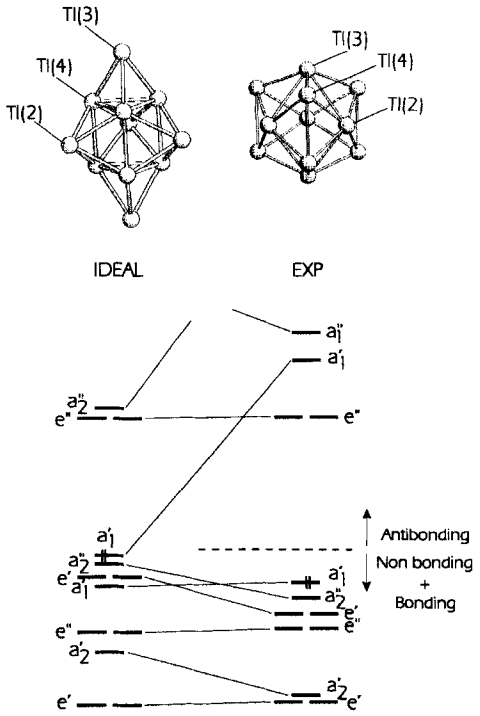

Figure 4. Molecular orbital correlation diagram for the distortion from the ideal pentacapped trigonal prismatic geometry to that of the experimentally observed cluster. This diagram shows the nine highest occupied MOs, which contain the 18 skeletal electrons. Labels correspond to the D_{3h} point group.

two three-center two-electron bonds. This is depicted in Figure 5 (the contribution of the three Tl(2) capping atoms are not shown for clarity). Naively, one might expect that this would require the lowering of the total electron count by 4 electrons, and not the value of 2 indicated in the correlation diagram. However, the distortion also results in an increase in the Tl(4)-Tl(x)-Tl(4) bond angles (where $x = 2, 3$). In some way this process must account for the discrepancy of the 2 electrons between our naive picture and that suggested by the correlation diagram.

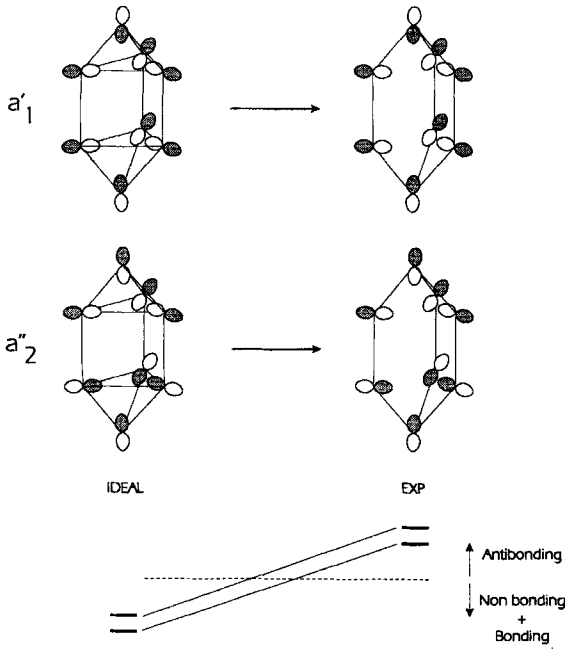

Figure 5. Illustration of the breaking of two three-center two-electron bonds within the ideal pentacapped trigonal prismatic Tl_{11}^{9-} cluster. For simplicity, the contributions of the three Tl(3) capping atoms have been omitted.

As one might expect, the elucidation of the above relationship between electron count and reorganization of Tl–Tl bonds is not simple, because of the rather delocalized nature of the cluster orbitals. The magnitude of the task can be reduced somewhat, since the orbitals of interest are not the full set of molecular orbitals, but rather the subset spanned by the a_1' and a_2'' representations of the D_{3h} point group. The reason for this is simple. Since the orbitals that should be going up in energy belong to this subset, this must also be true of the orbitals that cancel them out, owing to the noncrossing rule. Figure 6 depicts

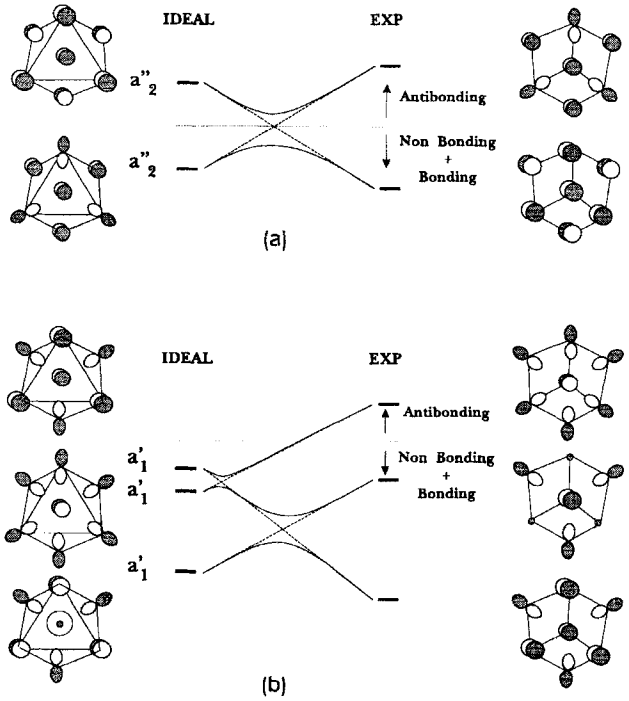

Figure 6. Correlation diagrams for the a_1' (a) and a_2'' (b) subsets.

the molecular orbital correlation diagrams for these two subsets as well as the relevant molecular orbitals. For clarity, the orbitals in Figure 6 have been drawn in a top view (see Scheme 1 for the top view of the cluster rearrangement). Inspection of this figure indeed reveals that the avoided crossing in the a_2'' subset leads to a lowering of electron count by two electrons instead of the four in the naive picture. The a_1' subset shows a rather complex system of avoided crossings, which finally leads to the expected raising of one orbital into the antibonding manifold.

We now turn to the question of whether these orbitals can be used to provide a simple interpretation of the above process. Consider the a_2'' subset, which contains two orbitals of interest (Figure 6a). The individual orbital correlations are indicated

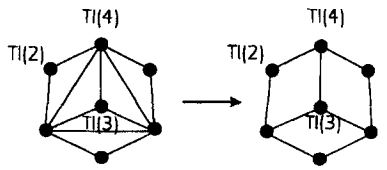

Scheme 1. Top view of the rearrangement of the Tl_{11}^{9-} cluster.

individual orbital correlations are indicated by the dotted lines in the correlation diagram of Figure 6a. The lower orbital is destabilized on going from the ideal to the real geometry, essentially because of the breaking of the three-center bonding involving the Tl(4) atoms. However, the raising of this orbital is counterbalanced by the lowering of a low-lying orbital of the same symmetry. The energy lowering of this orbital with the deformation to the real structure is a consequence of the change in the Tl(4)-Tl(x)-Tl(4) bond angles (where $x = 2$ and 3). The result is an avoided crossing, and one of the two orbitals representing the three-center bonding of Tl(4) atoms is not pushed up to the antibonding region. The correlation diagram for the a_1' subset is shown in Figure 6b. In this case there are three orbitals of interest and two avoided crossings. Although the upper filled a_1' orbital tries to decrease in energy when the ideal cluster starts to distort, there is an avoided crossing with the middle a_1' orbital, which results in a large increase in energy because of the breaking of the three-center bonding involving the Tl(4) atoms. In other words, there is no low-lying orbital of the same symmetry to interact with the upper orbital, which consequently moves into the antibonding orbitals region. Thus, only one of the two orbitals essentially describing the two three-center bonds of the Tl(4) atoms is really pushed up into the antibonding region. Although the highly delocalized nature of the orbitals makes it a little bit difficult to recognize, the increase in Tl(4)–Tl(4) distances essentially leads to the loss of two three-center bonds (i.e., loss of 4 electrons with respect to the ideal count), and the readjustment of the Tl(4)-Tl(x)-Tl(4) bond angles (where $x = 2$ and 3) allows the recovery of one electron pair.

Another angle on this problem is provided by the electron population analysis for the Tl_{11}^{7-} cluster reported in Table 4, which gives the total electron populations (TP), the number of electrons localized on a particular atom (i.e., on-site populations, OSP), and bond overlap populations. Here it should be recalled that the total electron density of an atom arises from two contributions in the Mulliken population analysis: 1) the on-site population or the electron density associated with a particular atom (i.e., the diagonal terms of the population matrix corresponding to this atom) and 2) half of the overlap populations associated with this atom (i.e., half of the nondiagonal terms of the population matrix, where one of the indices corresponds to one orbital of that atom). In other words, the total electron density can be considered to be the sum of the on-site electron density and of the electron density of this atom responsible for the bonding with other atoms (i.e., bonding electron density).

Table 4. Electron distribution and overlap population for the ideal pentacapped trigonal prismatic (ideal) and experimentally found (exp) Tl_{11}^{7-} clusters. TP and OSP refer to the *total* and *on-site* electron populations, respectively.

a) Electron distribution.

	Ideal		Experimntal	
	TP	OSP	TP	OSP
Tl(2)	4.47	3.25	3.32	2.14
Tl(3)	3.85	2.91	3.54	2.22
Tl(4)	3.15	1.92	3.82	2.72

b) Number of bonds and their overlap populations.

	Number of bonds		Overlap population	
	Ideal	Exp.	Ideal	Exp.
Tl(4)-Tl(4)	3	3	0.23	0.56
Tl(4)-Tl(4)	6	0	0.20	–
Tl(4)-Tl(2)	12	12	0.61	0.50
Tl(4)-Tl(3)	6	6	0.63	0.65
Tl(3)-Tl(2)	0	6	–	0.23

Taking into account the number of bonds of each type and the associated overlap populations, it is clear from the results of Table 4 that the *total* bonding electron density of the Tl_{11}^{7-} cluster in the two geometries is practically the same. What distinguishes the two geometries is the on-site electron densities of the three thallium atoms. Looking at both the total and on-site electron densities, it is clear that the three thallium atoms have similar electron densities in the experimental structure, but quite different ones in the ideal structure. In other words, the three thallium atoms would have different formal valences in the ideal structure, but not in the experimental one. Thus, it can be said that the Tl_{11}^{7-} cluster chooses the geometry with the more regular distribution of electron density among the different thallium atoms while maintaining the same total bonding population. With two extra electrons (i.e. the Tl_{11}^{9-} cluster) and the same geometry, antibonding orbitals would be filled and there would be a substantial decrease in bonding population. This is not the case for the pentacapped trigonal prismatic geometry (see Figure 4). Thus, in contrast to Tl_{11}^{7-}, Tl_{11}^{9-} will choose this geometry because it leads to the more favorable bonding population.

We will now explore one final aspect of this cluster geometry. In the experimental Tl_{11}^{7-} cluster the Tl(2)–Tl(3) bonds are relatively short (3.416 Å). This raises the question as to whether the square face of the cluster [Tl(3)-Tl(4)-Tl(2)-Tl(4)] should be viewed as a butterfly arrangement of two triangular faces (as shown in Figure 4, for instance) or as a square face. The calculated overlap population (Tl(3)–Tl(2) = 0.23 as compared to Tl(4)–Tl(4) = 0.56, Tl(4)–Tl(2) = 0.50, Tl(4)–Tl(3) = 0.65) suggests that the first description may be better, since the Tl(2)–Tl(3) bond has a sizeable overlap population. An investigation into the role of this bond was carried out by setting the Hamiltonian and overlap matrix elements (H_{ij} and S_{ij}, respectively) equal to zero when i and j were orbitals of the Tl(3) and Tl(2) atoms. The removal of these interactions provided only a small energy increase in the HOMO and almost no change in any other MO. In essence, the HOMO was raised by approximately 0.2 eV to the energy of a nonbonding Tl p orbital. The initial overlap population in the bond progressively disappears and becomes strongly localized on the Tl(3) site as the interactions between Tl(3) and Tl(2) are decreased. Thus, although the Tl(3)–Tl(2) "bonds" have a sizeable population, there is little energetic stability associated with their existence. Although this result may appear to be surprising, it is a reminder of the care that must be taken with the results of a Mulliken population analysis when the atoms possess very diffuse orbitals, as is the case for Tl. Thus we conclude that these "bonds" are not of great importance, and the structure is best viewed as containing six open square faces.

B. The Cd_9Tl_{10} sheet: The electron count for the cluster allows the chemical formula of the sheet to be evaluated as $Cd_9Tl_{10}^{7-}$. The nature of this sheet may now be investigated. The band

0947-6539/97/0305-0804 $ 17.50+.50/0 Chem. Eur. J. 1997, 3, No. 5

structure near the Fermi level is shown in Figure 7. It is clear from this figure that several dispersive bands cross the Fermi level so that the system should be metallic. In order to test this conclusion, the electrical resistivity of single crystals of $K_{14}Cd_9Tl_{21}$ were measured. In agreement with our prediction

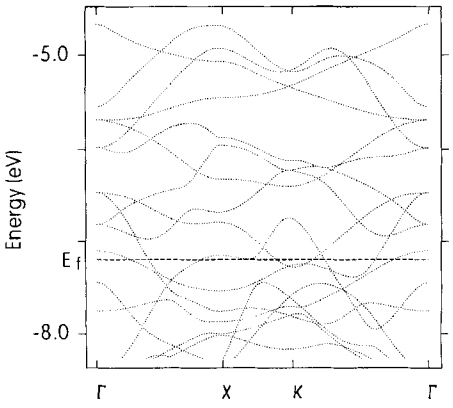

Figure 7. Calculated band structure for the $Cd_9Tl_{10}^{7-}$ sheet. Only the bands near the Fermi level are shown. The Γ, X, and K labels represent the (0,0), ($a^*/2$,0) and ($a^*/3$,$a^*/3$) wave vectors of the hexagonal Brillouin zone.

an overall metallic behavior between 218 and 323 K ($\rho \approx 4 \times 10^{-4}\ \Omega$cm at 295 K with a weak positive coefficient) was observed. Since several bands cross the Fermi level, the calculated Fermi surface is quite complex and not very informative, so that it is not reported here. The only interesting result in the context of the present work is that the system should be a highly isotropic two-dimensional metal. Thus, it is not expected that a Fermi surface driven instability will partially or totally destroy the Fermi surface and lead to some resistivity anomaly at low temperatures, as found in many low-dimensional metals.[33–34]

The question arises as to whether the metallic behavior of this slab can be attributed to a particular structural feature[35] or whether the entire slab should be considered as a delocalized metal. Inspection of the density of states at the Fermi level shows that each thallium and cadmium atom of the sheet makes a considerable contribution. This provides strong evidence for a highly delocalized system. Table 5 lists the reduced overlap populations between atoms in the sheet as well as their electron densities. Although it is clear from Table 5 that the cadmium atoms have more electron density associated with their position, the overall electron distribution is quite evenly spread over the sheet. Also, Table 5 shows that there is not only strong Cd–Cd bonding and Cd–Tl bonding, but also strong Tl–Tl bonding, which implies that a picture based on edge-sharing Cd–Tl clusters is not altogether appropriate. Thus, both the electronic states near the Fermi level and the bonding as a whole are fairly well delocalized over the entire sheet, and a view of this material based on the condensation of Cd–Tl clusters, although very useful as a structural description, does not seem to be quite appropriate from the electronic viewpoint.

Table 5. Bond lengths (Å), overlap populations, and electron densities calculated for the $Cd_9Tl_{10}^{7-}$ sheet.

Bond	Bond length	Overlap population	Atom	Electron density
Tl(1)–Tl(1)	3.686	−0.0398	Cd(1)	2.89
Tl(1)–Tl(5)	3.183	0.5386	Cd(2)	3.33
Tl(1)–Cd(1)	3.180	0.2232	Tl(1)	2.67
Tl(1)–Cd(1)	3.244	0.1297	Tl(5)	2.91
Tl(1)–Cd(2)	2.964	0.4215		
Tl(5)–Cd(1)	3.354	0.1798		
Cd(1)–Cd(2)	2.997	0.2045		
Cd(2)–Cd(2)	2.816	0.3829		
Cd(1)–Cd(1)	2.961	0.2180		
Cd(1)–Cd(1)	3.083	0.1441		

Finally, we considered the possible parameter dependence of our analysis. As mentioned above, two quite different parameter sets for Tl have been used in the literature (see Table 3). Obviously, the use of one or the other set does not have any great influence on the calculations for the isolated Tl_{11} cluster. However, this may not be true for the $Cd_9Tl_{10}^{7-}$ sheet. Based on the calculations using the second set of parameters for Tl, the material is found to be a highly isotropic two-dimensional metal; all the Tl and Cd atoms contribute considerably to the density of states at the Fermi level, and the Cd–Cd, Tl–Tl, and Cd–Tl overlap populations are very similar to those of Table 5. As expected from the considerably lower valence state ionization potentials of Tl 6p orbitals, the total electron density calculated for the Tl atoms is larger than that of the Cd atoms. However, the electron density continues to be fairly evenly distributed within the sheet. The main conclusions of our study remain valid when the second set of parameters for Tl is used, and we conclude that, in essence, our analysis is not parameter dependent.

As a final test we carried out a complete calculation[36] where the full three-dimensional structure of $K_{14}Cd_9Tl_{21}$ was used. This calculation clearly showed, at least within the context of the extended Hückel method, that 1) the Tl–K interactions are very weak (overlap populations of the order of 0.037) and 2) there is no appreciable electronic transfer between the Tl_{11}^{7-} and $Cd_9Tl_{10}^{7-}$ layers. In other words, it is the stability of the Tl_{11}^{7-} cluster that governs the electron distribution in this phase. Thus, it is suggested that the interactions between the three different types of layers of the structure are essentially electrostatic in nature.

Acknowledgements: R. R. would like to thank the NSERC of Canada for a postgraduate research fellowship.

Received: October 22, 1996 [F 505]

[1] M. L. Fornasini, M. Pani, *J. Alloys Compd.* **1994**, *205*, 179.
[2] R. Henning, J. D. Corbett, unpublished results, cited in ref. [10].
[3] C. Belin, *Acta Crystallogr.* **1980**, *B36*, 1339.
[4] M. Tillard-Charbonnel, N. Chouaibi, C. Belin, J. Lapasset, *Eur. J. Solid State Inorg. Chem.* **1992**, *29*, 347.
[5] K. Wade, *Adv. Inorg. Chem. Radiochem.* **1976**, *18*, 1.
[6] U. Franck Cordier, G. Franck Cordier, H. Schäfer, *Z. Naturforsch.* **1982**, *37b*, 119.
[7] U. Franck Cordier, G. Franck Cordier, H. Schäfer, *Z. Naturforsch.* **1982**, *37b*, 127.
[8] R. G. Ling, C. Belin, *Acta Crystallogr.* **1982**, *B38*, 1101.
[9] C. Belin, M. Tillard-Charbonnel, *Prog. Solid State Chem.* **1993**, *22*, 59.
[10] J. D. Corbett in *Chemistry, Structure and Bonding of Zintl Phases and Ions* (Ed.: S. Kauzlarich), VCH, in press.
[11] W. Blase, G. Cordier, M. Somer, *Z. Kristallogr.* **1991**, *194*, 150.
[12] Z. C. Dong, J. D. Corbett, *Inorg. Chem.* **1996**, *35*, 3107.
[13] D. A. Hansen, J. F. Smith, *Acta Crystallogr.* **1967**, *22*, 836.
[14] Z. C. Dong, J. D. Corbett, *J. Am. Chem. Soc.* **1994**, *116*, 3429.
[15] G. Cordier, V. Müller, *Z. Kristallogr.* **1992**, *198*, 281.
[16] G. Cordier, V. Müller, *Z. Naturforsch.* **1994**, *49b*, 935.

[17] Z. C. Dong, J. D. Corbett, *J. Am. Chem. Soc.* **1995**, *117*, 6447.
[18] M. M. Tillard-Charbonnel, C. H. E. Belin, A. P. Manteghetti, D. M. Flot, *Inorg. Chem.* **1996**, *35*, 2583.
[19] Z. C. Dong, J. D. Corbett, *Inorg. Chem.* **1995**, *34*, 5042.
[20] Z. C. Dong, J. D. Corbett, *Inorg. Chem.* **1996**, *35*, 1444.
[21] M. Tillard-Charbonnel, A. Chahine, C. Belin, *Z. Kristallogr.* **1995**, *210*, 162.
[22] G. M. Sheldrick, *SHELX-76, Program for crystal structure determination*, University of Cambridge, Cambridge, England.
[23] G. M. Sheldrick, *SHELXS-86, Program for crystal structure solution*, Institut für Anorganische Chemie der Universität, Tammannstrasse 4, D-3400 Göttingen, Germany.
[24] G. M. Sheldrick, *SHELXL-93, Program for crystal structure refinements*, Institut für Anorganische Chemie der Universität, Tammannstrasse 4, D-3400 Göttingen, Germany.
[25] a) L. Pauling, *J. Am. Chem. Soc.* **1947**, *69*, 542 b) *Proc. R. Soc. (London)*, **1949**, *A 196*, 343.
[26] a) R. Hoffmann, *J. Chem. Phys.* **1963**, *39*, 1397; b) M.-H. Whangbo, R. Hoffmann, *J. Am. Chem. Soc.* **1978**, *100*, 6093; c) A modified Wolfsberg–Helmholz formula was used to calculate the nondiagonal H_{ij} matrix elements: J. H. Ammeter, H.-B. Bürgi, J. Thibeault, R. Hoffmann, *J. Am. Chem. Soc.* **1978**, *100*, 3686.
[27] C. Janiak, R. Hoffmann, *J. Am. Chem. Soc.* **1990**, *112*, 5924.
[28] D. B. Kang, D. Jung, M. H. Whangbo, *Inorg. Chem.* **1990**, *29*, 257.
[29] H. Mercier, Y. Mathey, E. Canadell, *Inorg. Chem.* **1987**, *26*, 963.
[30] a) S. C. Sevov, J. D. Corbett, *Inorg. Chem.* **1991**, *30*, 4877; b) Z.-D. Dong, J. D. Corbett, *J. Cluster Sci.* **1995**, *6*, 187; c) Z.-D. Dong, J. D. Corbett, *Inorg. Chem.* **1996**, *35*, 1444.
[31] W. Blase, G. Cordier, V. Müller, U. Häußermann, R. Nesper, M. Somer, *Z. Naturforsch.* **1993**, *48b*, 754.
[32] R. Llusar, A. Beltrán, J. Andrés, B. Silvi, A. Savin, *J. Phys. Chem.* **1995**, *99*, 12483.
[33] J. A. Wilson, F. J. DiSalvo, S. Mahajan, *Adv. Phys.* **1975**, *24*, 117.
[34] E. Canadell, M.-H. Whangbo, *Chem. Rev.* **1991**, *91*, 965.
[35] See, for instance, our analysis of the origin of the metallic properties of LiZnGe: S. Sportouch, C. Belin, M. Tillard-Charbonnel, M. C. Rovira, E. Canadell, *New. J. Chem.* **1995**, *19*, 243.
[36] See the analysis of interactions of anionic species with alkali metal cations in: S. Alvarez, F. Mota, J. Novoa, *J. Am. Chem. Soc.* **1987**, *109*, 6586.

0947-6539/97/0305-0806 $ 17.50+.50/0